

# Appearance Fusion of Multiple Cues for Video Co-localization

Koteswar Rao Jerripothula, *Member, IEEE*,

**Abstract**—This work addresses a problem named video co-localization that aims at localizing the objects in videos jointly. Although there are numerous cues available for this purpose, for example, saliency, motion, and joint, their robust fusion can be quite challenging at times due to their spatial inconsistencies. To overcome this, in this paper, we propose a novel appearance fusion method where we fuse appearance models derived from these cues rather than spatially fusing their maps. In this method, we evaluate the cues in terms of their reliability and consensus to guide the appearance fusion process. We also develop a novel joint cue relying on topological hierarchy. We utilize the final fusion results to produce a few candidate bounding boxes and for subsequent optimal selection among them while considering the spatiotemporal constraints. The proposed method achieves promising results on the YouTube Objects dataset.

**Index Terms**—fusion, mixture, co-localization, video, GMM, appearance.

## I. INTRODUCTION

Automatic localization of commonly occurring objects in videos, also known as video co-localization, is a very challenging task. It is a critical problem in the computer vision research because it encodes the prerequisite ‘where’ for the generic ‘what’ and ‘how’ tasks such as object recognition [1] and action discovery [2], [3]. Recent deep learning studies have advanced the relevant research greatly, but a limited amount of annotated training data often constrains them. To ease the data annotation constraint, weakly supervised approaches [4], [5], [6], [7], [8] have attracted increasing interest in recent years. In this paper, we develop a weakly supervised approach, specifically focusing on localizing the commonly occurring primary objects in videos. By weakly-supervised approach, we mean that it requires weaker annotation (video label) than the expected output (bounding box).

There are a few exciting challenges that dynamic videos pose compared to the static images for effectively solving this problem of co-localization. First, there is an increased data volume (many frames in a video compared to single in an image). Moreover, there are many near-duplicates for each frame. Note that both the foreground similarity and the background variation are essential for effective co-localization. It is called variation vs. similarity issue in these joint frameworks since it’s not readily known what’s the foreground and the background. While the near-duplicates case is a rare phenomenon in images, it is not so in the case of videos. The near-duplicates issue makes it quite challenging to find suitable neighbors for

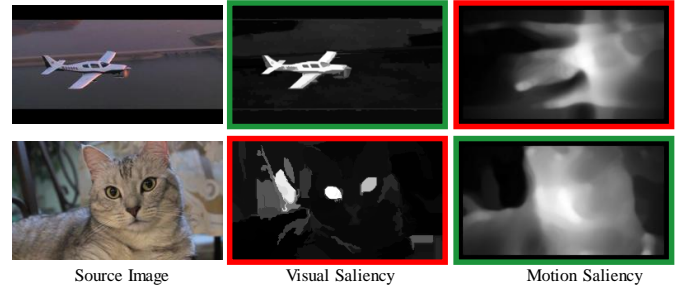


Fig. 1. Here are a few examples where available cues are spatially inconsistent. There are very few pixels which have similar likelihoods (foreground or background). The green bordered ones are readily good, whereas red ones are bad for dominant object localization. Why should we fuse good ones with bad another? Such questions rises a legitimate reliability issue while fusion multiple cues.

video frames because the nearest-neighbors approach, usually taken for images, would deem these near-duplicates as their neighbors. There would be hardly any background variation then. Thus, these contradicting requirements make reliance on the nearest neighbors approach problematic. Second, as we can see in Fig. 1, although videos, compared to images, are facilitated with motion saliency cues [9] in addition to the visual saliency cues [10], fusing them can be quite challenging, for the lack of spatial consensus on likelihoods. There are very few pixels which have similar likelihoods (foreground or background). Such spatial inconsistencies (lack of spatial consensus) are quite likely to happen because these priors have very different goals during their development. We can also observe in the figure that green-bordered ones are readily good; one may wonder if we should bother to fuse them with the bad other? This observation raises reliability issues also while fusing. The situation becomes further complicated when another cue, namely co-saliency as learned through weak supervision, is also brought into the picture. Third, the spatiotemporal constraints, such as edge awareness and smoothness, must also be taken into consideration in the video individually while co-localizing the objects in videos collectively.

Previously, [11], [12] dealt with the above challenges by sampling the frames, discovering the objects in the sampled frames, tracking the objects discovered, fusing the cues spatially, and selecting optimal generic object proposals. There are a few problems with these approaches. Firstly, essential changes in the non-sampled frames may miss out. Therefore, a method to handle all the frames is required. In this paper, we accomplish this through a topological-hierarchy approach.

K. R. Jerripothula is with the Department of Computer Science and Engineering, IIT Delhi, New Delhi, Delhi, 110020 India e-mail: (see <http://www.michaelsell.org/contact.html>).

The reason for using topological-hierarchy is that we can now exploit topological relations (i.e., the properties preserved through deformations) for generating co-saliency maps at multiple levels of the hierarchy having varying degrees (from high to low) of both the variation and the similarity. We can then strategically combine these co-saliency maps at various levels for the development of the final issue-free co-saliency map.

However, the nearest neighbor approach, generally used for images, would deal with only one degree in the case of videos: very low variation and very high similarity due to near-duplicates. In this way, the topological-hierarchy approach allows us to use any image co-saliency methodology on the video frames, which is otherwise tricky due to the presence of near-duplicates. Secondly, fusing different cues spatially without addressing inconsistency and reliability issues can prove to be detrimental. Therefore, there should be a way to evaluate and incorporate consensus and reliability constraints into the fusion process. Instead of fusing different priors in the spatial domain like in [11], in this paper, we explore the appearance domain where we merge different appearance models generated from the priors into one appearance model. There are also some works [13], [12] that combine these priors as energy terms with the help of trade-off parameters in their energy functions; however, parameter settings usually need to be varied according to the nature of the video. We can attempt to automate this process, maybe by incorporating the constraints discussed: the consensus between the priors and reliability of each of the priors. Lastly, note that the generic object proposals, generally used for these problems, are learned over limited categories; this very much limits the capability of weak supervision when applied to other categories. Therefore, in this paper, we try to generate proposals using the fusion result itself, which has benefited from weak supervision. Once generated, they also need to be selected while accounting for spatiotemporal constraints, as studied in [14], [13]. For instance, [13] develops spatiotemporal saliency prior for segmentation. However, in our case, since we build our final localization step centered around the fusion result itself, we design our spatiotemporal constraints accordingly.

Specifically, our approach is to fuse different cues in the appearance domain while accounting for consensus and reliability constraints. We merge them as appearance models. We use GMM (Gaussian Mixtures Model) for modeling the appearance. While we keep the distribution parameters of GMM components intact while fusing, we incorporate consensus and reliability constraints into the computation of their weights. The fused appearance model yields the required fusion result as a rough object mask. The three cues which we fuse in this paper are co-saliency, visual saliency, and motion saliency. While we propose a novel topological hierarchy based co-saliency cue, we use the existing methods [10], [9] for generating the remaining ones, respectively. We create a topological hierarchy through repeated clustering. First, we cluster all the frames in the dataset, then their representatives are clustered, and so on. We use image co-saliency generation algorithms to generate co-saliency maps at multiple levels, which are then combined to generate the required co-saliency

cue. Our final localization step is fusion-result centric, where we generate the proposals and score them based on the fusion result itself. They are selected based on these scores while respecting our spatiotemporal constraint on proposal coordinates. Our experiments demonstrate that the proposed method achieves better results compared to the state-of-the-art video co-localization methods on the YouTube Objects dataset.

The main contributions of this paper are threefold: 1) fusion of multiple cues in the appearance domain; 2) topological hierarchy based co-saliency approach to allow usage of existing image co-saliency algorithms in videos while tackling the issue due to near-duplicates; 3) mask-centric proposal generation followed by spatiotemporally constrained optimization for localization.

## II. RELATED WORKS

### A. Co-saliency

The work in [15] uses the co-saliency cue effectively in the co-segmentation problem. A cluster-based co-saliency method was proposed in [16], where the developed cues are fused spatially. As far as videos are concerned, the term video co-saliency (different from video saliency[17]) was introduced by [18] to eventually to video co-segmentation while integrating different saliency cues. An interesting way of generating such cues, using object proposals, was proposed in [19]. Other similar fusion approaches [20], [21] fuse raw saliency maps of different images to generate co-saliency maps. To the best of our knowledge, only [22], [23] are related to hierarchy based co-saliency detection. Our topological hierarchical co-saliency idea is quite different. While the hierarchy represented in [23] depicts different scales of the image, the hierarchy in this paper depicts different topological levels of the dataset. And while [23] uses hierarchical segmentation [24] to obtain the co-saliency, we use existing co-saliency idea to obtain topological hierarchy based co-saliency.

### B. Co-localization

Co-localization, similar to co-segmentation, uses multiple images but to output bounding box around the object. It was introduced by [25]. Initially, image co-localization methods were developed, such as [25], [26], [27], later extended to video co-localization methods. For example, the image co-localization method [25] was extended to the video co-localization method [28], where a quadratic optimization-based framework was proposed. The image co-localization method [26] extends to the video co-localization method [11], where the authors propose a spatial fusion-based approach using the raw saliency maps. Then, an unsupervised image co-localization method [27] extends to a video co-localization method [12], which can localize the dominant objects even without necessarily requiring the image or video labels.

Specifically, [28] and [29] are two frameworks that jointly locate common objects across the videos all at once. In [28], it used the quadratic programming framework to co-select bounding box proposals in all the video frames together. While in [29], it formed candidate tubes and co-selected tubes across the videos to locate the shared object. Recently,

[12] proposed to develop foreground confidence for bounding boxes and select optimal ones while maintaining temporal consistency. However, it is a computationally intensive method requiring to match hundreds of proposals for a large number of frames of different videos. [11], [30] propose an efficient way by proposing co-saliency activated tracklets that locates the objects individually through co-saliency developed jointly for some sampled frames. However, such an approach may miss some significant changes that occur in the non-activators (non-sampled frames).

In contrast, we make up for this limitation by building a topological hierarchy on all the frames. Furthermore, we fuse appearance models instead of maps of cues, as performed in [11], [30]. [31] reports improved co-localization in videos by using certain pre-trained deep learning networks and motion cues. However, such approaches are limited to the categories that the pre-trained network has seen during the initial training process.

### III. PROPOSED METHOD

#### A. Overview

Our main goal is to fuse different priors (co-saliency, visual saliency, motion saliency) in the appearance domain while incorporating consensus and reliability constraints into the fusion process. We do this for generating rough object masks required for localizing the objects. Our proposed method is as follows. First, since we cannot directly use image co-saliency methods for generating video co-saliency due to near-duplicates, we develop topological hierarchical co-saliency to allow image co-saliency methods to generate video co-saliency also. Second, with the availability of the three priors, we generate different appearance models *via* their tri-maps and fuse them to make one appearance model. This new appearance model is used to create a rough object mask. Third, we conduct localization entirely based on the obtained rough object mask. We use it to generate the proposals, score them, and use their coordinates to enforce spatiotemporal constraints.

#### B. Co-saliency Generation

We develop a topological hierarchy for generating co-saliency cues. The topological hierarchy of video frames provides us a multi-level representation of topological relationships existing in the dataset. Such a representation facilitates the strategic exploitation of multi-level co-saliency maps to generate a final one. Denote such a dataset as  $\mathcal{V} = \{V_1, V_2, \dots, V_n\}$  having total  $n$  videos. Let each video be denoted as  $V_i = \{F_i^1, F_i^2, \dots, F_i^{|V_i|}\}$ , i.e., set of the comprising frames.

We build our topological hierarchy of frames in the following manner: At the ground level (denoted as  $\mathcal{F}_0$ ), all the video frames are present. At a level higher than  $\mathcal{F}_0$  is  $\mathcal{F}_1$ , where the representatives of  $\mathcal{F}_0$  are present. Similarly,  $\mathcal{F}_2$  consists of representatives of  $\mathcal{F}_1$ , and so on. Note that in Fig. 2 GIST [32] (a global descriptor) variation (in brackets) increases as we go to the higher level in the hierarchy of topological representative frames. The GIST variation here means variance of GIST features of the frames present on a

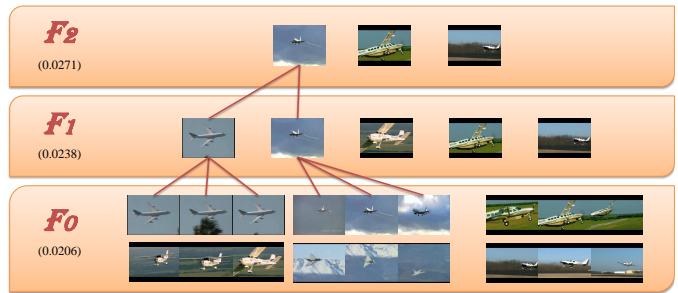


Fig. 2. An illustration of topological hierarchy development: A higher level comprises of representatives of frames at lower level. And as we go higher, the variation (encoded in variance) increases.

particular level of the hierarchy. We choose frames nearest to the k-means cluster centers as the representative frames. We adjust the number of clusters in a manner that there are 15 frames on an average in a cluster. The hierarchy building is terminated when the variation is above a certain threshold, or the number of representatives is less than a minimum number (i.e., the desired average number of frames in a cluster: 15).

Once we generate the hierarchy, we can now use an image co-saliency technique in [20] to generate co-saliency maps at multiple levels using the frames available at the lower levels. Now, the idea behind image co-saliency in [20] is to warp saliency maps of other images to the representative image first and then to propagate these generalized co-saliency maps to other images by warping them back for obtaining their co-saliency maps. [20] used only a two-level hierarchy. In our case, since we have multiple levels, we start from the lowest level and generate co-saliency maps at each level progressively using the co-saliency maps (saliency maps in the case of  $F_1$  because there are no co-saliency maps yet for the for  $F_0$ ) of the lower level, up to the highest one. The idea is to witness the varying degrees of similarity and variation at multiple levels, and benefit from all, not just the bottom-most level ( $F_0$ ), a kind of nearest neighborhood approach.

Now, with co-saliency maps available at multiple levels (except  $F_0$ ), as far as propagation is concerned, we start disseminating from the highest level generating a new co-saliency map at each level for ultimately yielding the co-saliency maps of  $F_0$ . For this propagation step, we set the weights for the fusion of disseminating warped saliency maps and the current co-saliency map (saliency map for  $F_0$ ) at a particular level to the number of levels covered so far while propagating and one, respectively. Such a weight-assignment appropriately acknowledges the importance of disseminating warped co-saliency maps over the current one. In this way, we can eventually generate final co-saliency maps at  $F_0$  level as well, which had only saliency maps at the beginning. Now that co-saliency cue required for appearance fusion (to be discussed in the next section) is available for each frame, let us denote the developed co-saliency cue as  $P_c$  for a frame.

Essentially, in the topological hierarchy co-saliency approach, we have extended the [20] co-saliency method for its application on video frames by applying it at multiple levels,

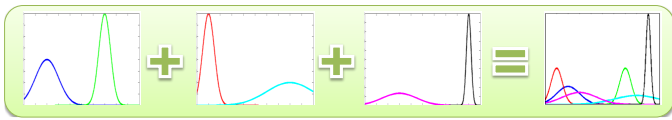


Fig. 3. A representation of our appearance fusion idea, where we stack the components of different appearance models into one appearance model. Note how the distribution parameters of different components (means and variances) just get transferred here. Similarly, the distributions parameters of our GMM components also just get transferred to create the new appearance model.

instead of just two, of our hierarchy.

### C. Appearance Fusion

In the previous sub-section, we developed co-saliency cue ( $P_c$ ), which we fuse with the existing visual-saliency (denoted as  $P_v$ ) [10] and motion saliency (denoted as  $P_m$ ) [9] cues. These cues are effective in different scenarios. For example, (i) in simple backgrounds, visual saliency itself is sufficient; (ii) in complex backgrounds, the jointly-processed co-saliency prove to be more effective than visual saliency; (iii) in the case of unique motion of the moving objects, the motion saliency is more effective regardless of whether the background is simple or complex. However, none of them is foolproof. Intuitively, we should combine them for better object discovery [33]; however, they are usually inconsistent, and fusion can perform worse than when used individual at times. The reason behind such spatial inconsistency is that any individual cue has its own goal. Therefore, we explore the appearance domain for the fusion of these priors. In the appearance domain, we deal more with global appearance than local details. The idea here is to fuse the appearance models developed from these priors into one new appearance model. Firstly, we created tri-maps from the priors. From these tri-maps, we generated respective appearance models. We then stacked all the foreground GMM components into one new foreground GMM and all the background GMM components into one new background GMM as shown in Fig. 3.

In essence, we assign the distribution parameters of existing components to the distribution parameters of components of new GMMs. However, we cannot just transfer the weights for these components; they need to be determined. These weights can be seen as fusion weights in the appearance domain. To facilitate the computation of these weights, we create a map called consensus aware reliability score map for incorporating our consensus and reliability constraints. We develop the map using the signed sum of reliability scores of the cues at the pixel level. The signs account for consensus amongst the priors for each pixel. Therefore, it results in a map that takes into account both the constraints. The weights of the components are computed as average scores of the components' pixels in the map. In this way, we create a new appearance model, which is ready to be used for segmenting out the object roughly.

Let the set of cues be denoted as  $\mathcal{P}$ . In the current problem context,  $\mathcal{P} = \{P_k | k = c, v, m\}$ . Let  $I$  be the frame into consideration along with its pixel domain  $D$ .

**GMM:** In order to develop GMMs, we need tri-maps, which are developed in the following way. For a cue  $k$ , let

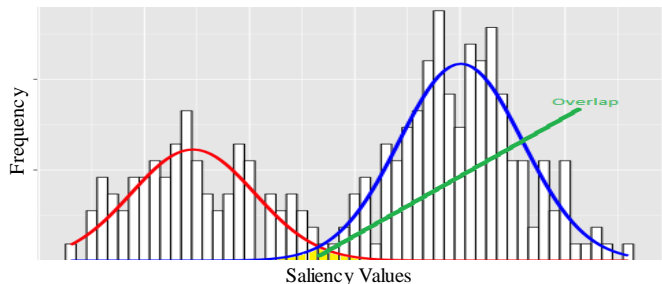


Fig. 4. The reliability scores are developed using the computed overlap between Gaussian fits of foreground and background distributions (developed through Otsu thresholding). The lesser the overlap, the more the reliability score.

$T_k = \{T_k^f, T_k^b, T_k^u\}$  be the tri-map, where superscripts ( $f, b, u$ ) denote foreground, background and unspecified regions of the tri-map and their corresponding labels in the tri-map are 1, -1 and 0, respectively. If  $p$  denotes a pixel, it gets assigned to a particular region of  $T_k$  based on the following criterion:

$$p \in \begin{cases} T_k^f, & \text{if } P_k(p) > 0.7; \\ T_k^b, & \text{if } P_k(p) < \min(0.7, \phi_k); \\ T_k^u, & \text{otherwise;} \end{cases} \quad (1)$$

where  $\phi_k$  denotes Otsu threshold value of  $P_k$  for obtaining the background seeds. From these tri-maps, respective GMMs are modeled. Every GMM appearance model consists of  $C$  components (typically, 5, as suggested in the grabcut strategy [34]) each for the foreground and background distributions. We simply mix these components of different GMMs, separately for foreground and background, to create a new GMM. The new GMM now consists of total  $3 \times C$  components each for the foreground and background distributions. Each of these components are required to be appropriately weighted for effective object discovery through grabcut optimization [34]. In this way, we reduce the problem of fusion of cues in the spatial domain to the problem of fusion in the appearance domain.

**GMM weights:** In this section, we will discuss how we appropriately weight our appearance model (GMM) components. Any GMM (foreground/background) component holds three parameters: weights ( $\pi$ ), means ( $\mu$ ) and co-variances ( $\sigma$ ). While we keep the computation of  $\mu$ 's and  $\sigma$ 's same as in the grabcut optimization [34], we alter only the GMM weights. In the original Grabcut strategy, a pixel belonged to a single component; therefore, weights of these components were computed as the fraction of the spatial domain that belonged to the particular component. However, now a pixel belongs to multiple components (one from each cue), we design the weights differently. If  $G(c)$  denotes the subset of the spatial domain that belongs to the  $c^{th}$  component, i.e.,  $G(c) = \{D(p) | p \rightarrow c\}$ , we weight component  $c$  based on how well it supports this appearance fusion guided by reliability and consensus constraints. For this purpose, we use the map called consensus aware reliability map ( $X$ ) developed by us.

TABLE I  
COMPUTATION OF CONSENSUS AWARE RELIABILITY MAP  $X$  BASED ON LOCATION OF PIXEL IN DIFFERENT KINDS OF CONSENSUS REGIONS AMONG THE TRI-MAPS

S. No.	$X(p)(3)$	Cases
1 & 2	$(\psi(P_c) + \psi(P_v) + \psi(P_m))$	$p \in (T_c^f \cap T_v^f \cap T_m^f)$ or $(T_c^b \cap T_v^b \cap T_m^b)$
3 & 4	$abs\{\psi(P_v) + \psi(P_m) - \psi(P_c)\}$	$p \in (T_c^b \cap T_v^f \cap T_m^f)$ or $(T_c^f \cap T_v^b \cap T_m^b)$
5 & 6	$abs\{\psi(P_c) + \psi(P_m) - \psi(P_v)\}$	$p \in (T_c^f \cap T_v^b \cap T_m^f)$ or $(T_c^b \cap T_v^f \cap T_m^b)$
7 & 8	$abs\{\psi(P_v) + \psi(P_c) - \psi(P_m)\}$	$p \in (T_c^f \cap T_v^f \cap T_m^b)$ or $(T_c^b \cap T_v^b \cap T_m^f)$
9 & 10	$abs\{\psi(P_v) - \psi(P_m)\}$	$p \in (T_c^u \cap T_v^f \cap T_m^b)$ or $(T_c^u \cap T_v^b \cap T_m^f)$
11 & 12	$abs\{\psi(P_m) - \psi(P_c)\}$	$p \in (T_c^b \cap T_v^u \cap T_m^f)$ or $(T_c^f \cap T_v^u \cap T_m^b)$
13 & 14	$abs\{\psi(P_c) - \psi(P_v)\}$	$p \in (T_c^f \cap T_v^b \cap T_m^u)$ or $(T_c^b \cap T_v^f \cap T_m^u)$
15 & 16	$\psi(P_c)$	$p \in (T_c^f \cap T_v^u \cap T_m^u)$ or $(T_c^b \cap T_v^u \cap T_m^u)$
17 & 18	$\psi(P_v)$	$p \in (T_c^u \cap T_v^f \cap T_m^u)$ or $(T_c^u \cap T_v^b \cap T_m^u)$
19 & 20	$\psi(P_m)$	$p \in (T_c^u \cap T_v^u \cap T_m^f)$ or $(T_c^u \cap T_v^u \cap T_m^b)$
21 & 22	$(\psi(P_v) + \psi(P_m))$	$p \in (T_c^u \cap T_v^f \cap T_m^b)$ or $(T_c^u \cap T_v^b \cap T_m^b)$
23 & 24	$(\psi(P_c) + \psi(P_m))$	$p \in (T_c^f \cap T_v^u \cap T_m^f)$ or $(T_c^b \cap T_v^u \cap T_m^b)$
25 & 26	$(\psi(P_v) + \psi(P_c))$	$p \in (T_c^f \cap T_v^f \cap T_m^u)$ or $(T_c^b \cap T_v^b \cap T_m^u)$
27	0	$p \in (T_c^u \cap T_v^u \cap T_m^u)$

The GMM weight  $\pi(c)$  for  $c^{th}$  component is determined as the following:

$$\pi(c) = \frac{\sum_{p \in G(c)} X(p)}{|G(c)|} \quad (2)$$

where we essentially compute the weight of  $c^{th}$  component as the average score of the pixels that belonged to  $G(c)$ . In this way, we attain the weights required for fusion in the appearance domain. Note that since these weights need to sum to 1, we normalize these weights accordingly. We develop the consensus aware reliability map ( $X$ ) using

$$X(p) = abs\left\{\sum_{k=1}^{|\mathcal{P}|} T_k(p) \times \psi(P_k)\right\} \quad (3)$$

where we do the signed sum of reliability scores  $\psi(\cdot)$  of the priors for each pixel. By the signed sum, we mean coefficients could be 1, -1, or 0 depending upon pixel's value in a particular tri-map. Essentially, if the signs are similar for a particular pixel, there is a consensus. We design the equation such that: if the consensus is high, the score will also be as high as possible, and if the consensus is poor, the score will become as low as possible. Note that the reliability score  $\psi(\cdot)$  is computed using [20] for a given cue. [20] computes these reliability scores according to the overlap between Gaussian fits of foreground and background distributions (developed using the Otsu's threshold), as shown in Fig. 4. The lesser the overlap, the more the reliability score. The labels  $T_k(p) \in \{1, -1, 0\}$  of respective tri-maps form coefficients of these scores. Such design brings out both the consensus concept and reliability quite nicely: if they are reliable and they agree with each other in terms of their known labels, the score will be high. By known labels, we mean foreground (1) and background (-1) labels. Table I demonstrates all the possible values that we would obtain in  $X$  depending upon the different cases that arise with the available cues:  $P_c$ ,  $P_v$  and  $P_m$ . It can be seen that as the consensus reduces from top to bottom, the obtained score also decreases gradually. Note that we have united (using 'or') different cases in the table to save space if the same score

is obtained. A total of  $3^{|\mathcal{P}|}$  cases are possible if  $|\mathcal{P}|$  cues are available.

Since we are interested only in a rough object mask for localization, we consider the resultant mask of grabcut strategy with this modification after a single iteration itself as the required rough object mask. Note that the foreground pixels in the rough object mask may not be sufficiently accurate enough to effectively localize the video objects because we haven't yet examined the spatiotemporal constraints.

#### D. Masked Spatiotemporal Localization

In this section, firstly, we discuss how we generate several bounding box proposals using our rough object masks. Secondly, we discuss how we develop a graph using these proposals. Lastly, we discuss how we generate a single tube optimized over the graph.

**Bounding-Box Proposal Generation:** We build a bounding-box upon edge pixels of an object. We identify nearest edge pixels (from the edge map) of foreground pixels (from our rough object mask) as these edge pixels of the object. Specifically, we create distance-transform of the edge map and then find the nearest edges for foreground pixels of our mask. We use *vl\_imdisttf* function in *vlfeat* [35] library for this purpose. A reference bounding box is generated over the extreme edge pixels in the image, as shown in Fig. 5 to help in scoring candidate bounding box proposals generated from available edge pixels of the object. We consider only those bounding boxes as candidates that contain centroid of the foreground pixels and pass through sampled edge pixels (for efficient computation later on). The requirement of having centroid within the bounding box ensures limiting the candidates while respecting our object mask sufficiently. Denote  $\mathcal{B}_i^j$  as a set of such proposals in the frame  $F_i^j$ .

**Graph:** For any video, we construct a directed graph  $\mathcal{G} < H, L >$  which connects the bounding box proposals from adjacent frames as shown in the Fig. 6, where  $H$  denotes a set of all the bounding box proposals as nodes, and  $L$  denotes the set of linkages that connect the nodes. For simplified notations,





Fig. 5. Generation of bounding box proposals: (i) Using the distance transform of the edge map, we obtain the nearest edges of foreground pixels of rough object mask. (ii) We create a reference box using the extremes of these nearest edges. (iii) Several proposals generated using these nearest edges in a sampled manner such that the centroid of the foreground segment remain inside the proposal.

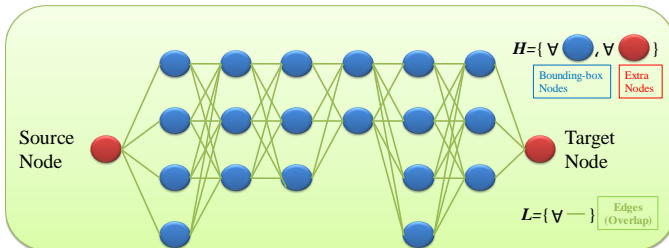


Fig. 6. Graph to represent the bounding boxes as nodes and overlaps as linkages.

let  $H$  and  $L$  also denote the sets of weights of nodes and edges, respectively. While its perimeter weights each proposal (node), the linkages between proposals of adjacent frames are weighted by Euclidean distance in terms of top, bottom, left, and right coordinates. Since the highest perimeter is possible only for our reference bounding box, the higher the perimeter means closer is the proposal to reference. And more the distance between proposals from adjacent frames, lesser is their overlap. We also add source and target nodes at the two ends of the graph to facilitate the formulation of the shortest path problem to select optimal proposals for localization of the objects.

**Objective Function:** The goal of the shortest path problem is to traverse a path from source to target at the lowest possible cost. Denote the edge selection variable and the node selection variable as  $\mathbf{z}$  and  $\mathbf{y}$ , respectively. Since the selection of edges inherently takes care of the selection of bounding boxes also, we formulate the objective function as

$$\begin{aligned}
 \min_{\mathbf{y}, \mathbf{z}} \quad & \sum_{(m,n) \in \mathcal{L}} \mathbf{y}_{mn} (-\log(H_m H_n) + \lambda L_{mn}) \\
 \text{s. t.} \quad & \sum_{k=1}^{|\mathcal{B}_i^j|} \mathbf{z}(j, k) = 1, \forall F_i^j \in V_i \\
 & \mathbf{y}_{mn} = \mathbf{z}_m = \mathbf{z}_n \\
 & \mathbf{y} \in \{0, 1\}, \mathbf{z} \in \{0, 1\}
 \end{aligned} \quad (4)$$

where intuition is that  $\mathbf{y}_{mn} \in \mathbf{y}$  indicates whether edge between nodes  $m$  and  $n$  (consequently the nodes also) will be part of the path or not. The cost for selecting a node-pair, computed as negative logarithm of the product of the node weights involved, encourages legitimate selection of proposals with higher parameter to signify our reliance on the mask. The cost for selecting an edge encourages linkages

having higher overlap between proposals involved to ensure a spatiotemporally smooth tube. The two costs are traded off by a parameter  $\lambda$ . Moreover, the objective function is subjected to the requirement of selecting one candidate bounding box per frame. Another requirement is that if a linkage is selected, nodes across them must also be selected. This objective function can be easily solved using Dijkstra's shortest path algorithm to compute  $\mathbf{z}$ , which gives the list of bounding boxes selected for localizing the object in each frame of the video  $V_i$ . There is a similar work [36] using shortest path algorithm in the joint processing research. However, there are two main differences: (1) In [36], the goal is image co-segmentation; therefore, local region proposals have been used. Each node represents a region proposal. In the proposed method, the goal is video co-localization; therefore, bounding box proposals have been used. Each node represents a bounding box proposal. (2) In [36], the weights computations are based on appearance feature similarity and saliency to select appearance-wise similar and salient region proposals. In this paper, weights computation is based on bounding box coordinates (top, bottom, left and right) similarity and perimeter of the bounding box proposal to select the proposals that are coordinates-wise similar across adjacent frames and are close to our reference bounding box generated from our appearance fusion results.

## IV. EXPERIMENTS

### A. Experimental Setup

We use the YouTube Objects dataset, which consists of 10 categories belonging to either animal (e.g., cow and cat) or vehicle (e.g., train and car). Each category has significant intra-class variation, making it a challenging dataset for video co-localization problem. We report our results using these annotations also. Following the literature, we use the CorLoc evaluation metric, i.e., the percentage of frames that satisfy the IoU (Intersection over Union)  $> 0.5$  condition.

### B. Video Co-localization Results

We evaluate the proposed technique under a weakly supervised setup. Under the weakly supervised setup, we build our topological hierarchy upon the videos of the same category by exploiting the category information. We report four types of results to demonstrate the importance of each of the proposed method's components. First, Avg.  $(P_v, P_m)$  denotes results obtained by averaging  $P_v$  and  $P_m$  (visual and motion saliency

TABLE II  
CORLOC RESULTS OF VIDEO CO-LOCALIZATION ON YOUTUBE-OBJECTS DATASET UNDER WEAKLY SUPERVISED SCENARIO.

	aeroplane	bird	boat	car	cat	cow	dog	horse	bike	train	avg
Prest et al. [29]	51.7	17.5	34.4	34.7	22.3	17.9	13.5	26.7	41.2	25.0	28.5
Joulin et al. [28]	25.1	31.2	27.8	38.5	41.2	28.4	33.9	35.6	23.1	25.0	31.0
Kwak et al. [12]	56.5	66.4	58.0	<b>76.8</b>	39.9	69.3	50.4	56.3	53.0	31.0	55.7
Jerri. et al. [11]	65.7	59.6	66.7	72.3	55.6	64.6	66.0	50.4	39.0	42.2	58.2
Avg. ( $P_v, P_m$ )	55.9	46.2	65.2	57.1	43.6	46.5	62.4	50.4	53.0	27.6	50.8
Avg. ( $P_c, P_v, P_m$ )	63.7	57.7	63.8	64.3	48.1	52.0	66.7	48.8	<b>55.0</b>	29.3	54.9
Appearance Fusion	69.9	61.5	63.0	68.8	57.9	68.5	69.5	56.6	54.0	39.7	60.9
Proposed Method	<b>70.9</b>	<b>67.3</b>	<b>72.5</b>	75.0	<b>59.4</b>	<b>73.2</b>	<b>70.9</b>	<b>57.4</b>	<b>55.0</b>	<b>51.7</b>	<b>65.3</b>

TABLE III  
IOU RESULTS OF VIDEO CO-LOCALIZATION ON YOUTUBE-OBJECTS DATASET UNDER WEAKLY SUPERVISED SCENARIO.

	aeroplane	bird	boat	car	cat	cow	dog	horse	bike	train	avg
Kwak et al. [12]	51.4	<b>59.5</b>	48.9	62.3	35.8	60.9	48.3	<b>50.4</b>	<b>49.0</b>	37.8	50.4
Jerri. et al. [11]	60.5	48.6	57.8	58.5	48.6	61.3	57.7	46.5	39.4	42.4	52.1
Avg. ( $P_v, P_m$ )	52.3	45.6	55.4	49.6	42.9	45.3	56.5	44.7	48.2	34.6	47.5
Avg. ( $P_c, P_v, P_m$ )	57.1	49.1	55.6	52.5	45.2	49.0	59.3	44.5	47.2	35.9	49.5
Appearance Fusion	<b>60.7</b>	51.1	54.3	55.6	50.6	59.2	<b>61.9</b>	48.9	48.5	41.9	53.3
Proposed Method	60.3	55.0	<b>58.2</b>	<b>63.5</b>	<b>54.2</b>	<b>64.1</b>	61.2	50.3	46.9	<b>45.2</b>	<b>55.9</b>

TABLE IV  
CORLOC RESULTS ON YOUTUBE-OBJECTS DATASET IN THE UNSUPERVISED MODE WHERE WE DO NOT USE VIDEO-LEVEL LABELS OF SEMANTIC CATEGORY. WE COMPARE THESE RESULTS WITH THAT OF TABLE II TO FIND THE DROP IN PERFORMANCE WHEN VIDEO-LEVEL LABELS OF SEMANTIC CATEGORY ARE MADE UNAVAILABLE.

	aeroplane	bird	boat	car	cow	cat	dog	horse	motorbike	train	avg	drop
Kwak et al. [12]	55.2	58.7	53.6	72.3	33.1	58.3	52.5	50.8	45.0	19.8	49.9	5.8
Jerri. et al. [11]	66.7	48.1	62.3	51.8	49.6	60.6	58.9	41.9	28.0	47.4	51.5	6.7
Ours (Unsupervised)	<b>70.3</b>	63.5	<b>70.3</b>	<b>74.1</b>	<b>52.6</b>	<b>70.1</b>	<b>73.1</b>	<b>58.9</b>	<b>57.0</b>	<b>50.0</b>	<b>64.0</b>	<b>1.3</b>

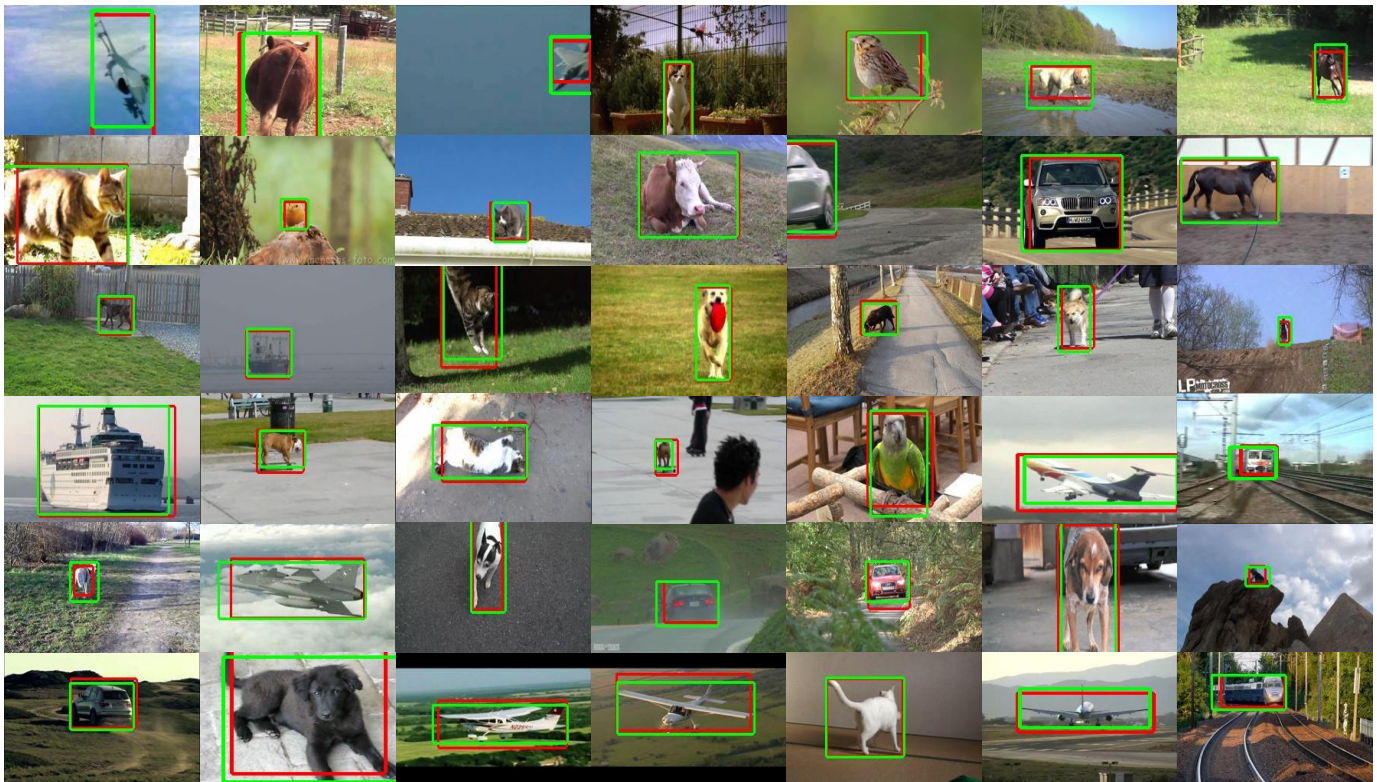


Fig. 7. Sample object localization results (red) in wide variety of video frames across the YouTube Objects dataset along with their corresponding ground truth bounding boxes (green). It can be seen that they are quite close.



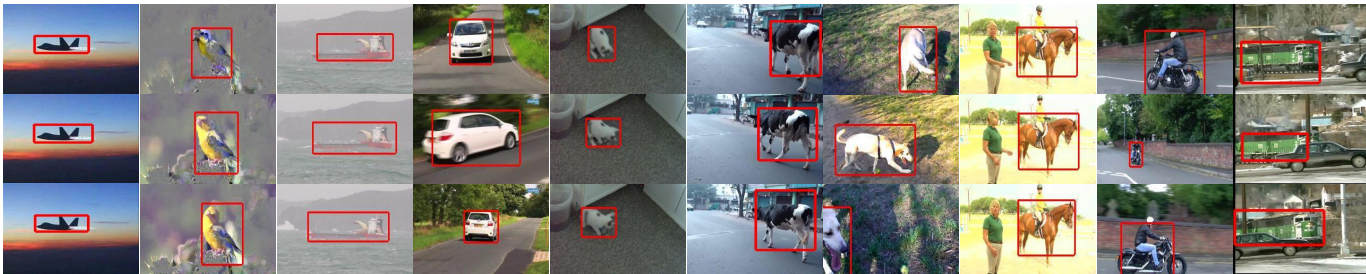


Fig. 8. Sample object co-localization results in different videos. The proposed method is able to accommodate variations of size, location, view, etc.

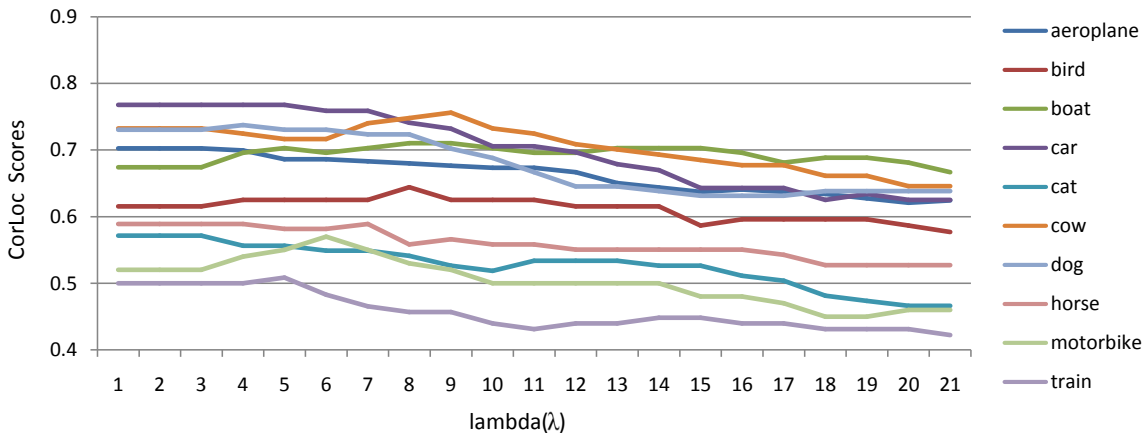


Fig. 9. The proposed method's category-wise performance variation with different  $\lambda$ .

cues); it's a baseline. Second,  $\text{Avg.}(P_c, P_v, P_m)$  denotes results obtained when we add the developed  $P_c$  to the first one. Third, we report the results obtained by the proposed appearance fusion scheme instead of averaging. In all these three types, we use a tight bounding box across the largest foreground component of a rough object mask for obtaining the results. Fourth, we report results obtained by our full method, where we consider the spatiotemporal constraints also.

It can be seen in Tables II-III that our method outperforms the existing state-of-the-art methods. We achieve around 12% and 7% relative improvement over [11] (the best so far) in terms of CorLoc and IoU metrics, respectively. From Table II, we can also note how each of our components progressively contributed: (i) upon introduction of  $P_c$ , the performance improves by 4.1%; (ii) upon introduction of appearance fusion, the performance improves by 6%; and upon introduction of SPL (i.e., the proposed method), there is further improvement of 4.4%. As far as our qualitative results are concerned, while Fig. 7 demonstrates the closeness of our results (red) to the ground truths (green), the Fig. 8 demonstrates the ability of our method to handle all kinds of variations within the video.

To show the effectiveness of our topological hierarchy-based neighborhood approach over nearest-neighborhood approach in video co-localization, we run different video co-localization methods in the unsupervised mode on the entire dataset, i.e., without using the video level labels of semantic category. In such a mode, the algorithm has to entirely rely on its

neighborhood building technique for jointly localizing the objects instead of human annotations of video-level labels of semantic category. The results are given in Table IV. We obtain 24% relative improvement over [11] in terms of the CorLoc metric. Note that after neglecting the video-level labels of semantic category in the unsupervised mode, our performance drops only slightly, from 65.3 to 64, which is just a drop of 1.3 CorLoc score. In contrast, there are drops of 6.7 and 5.8 CorLoc scores in the case of [11] and [12], respectively. Given such a lesser reduction in the drop when there is such an increase of diversity, it is clear that our topological hierarchy-based neighborhood approach provides a better neighborhood exposure compared to the nearest neighborhood-based approach (as adopted by [11] and [12]) for object discovery.

Additionally, when 15k ground truths annotated by [30] are used for evaluation, we obtain a CorLoc score of 63.0 compared to 53.5 of [30]. The noteworthy drop of 2.3 compared to the score obtained against 1.4k ground truths in Table II is due to the stricter evaluation with the increased number of annotations.

### C. Performance variation while varying $\lambda$

$\lambda$  is the only parameter in our model that gets introduced in the objective function (4). When varied in steps of one as in Fig. 9, it can be seen that for most categories performance remains decent for a good range (1-7) of  $\lambda$  and continuously deteriorates thereafter. This is because, as  $\lambda$  increases, the



model becomes overly dependent upon smoothness and neglects to rely on our rough object mask. This results in poor choice of proposals. We fix default parameter value of  $\lambda$  as 5 in our experiments.

#### D. Execution Time

Our algorithm takes about 9 hours and 17 hours for co-localizing the objects in the YouTube Objects dataset provided we sample one frame out of every 10 and 5 frames, respectively. It is comparable to the time taken by [11] (i.e., 16 hours) and significantly less compared to the time taken by [12] (i.e., 60 hours), which samples one frame out of every 20 frames.

### V. CONCLUSION

This paper proposes a novel approach for video co-localization through appearance fusion, where we fuse multiple cues as appearance models. Combined with other components of the proposed method, namely topological hierarchy based co-saliency and masked spatiotemporal localization, the proposed approach obtains state-of-the-art co-localization results on YouTube Objects dataset.

### REFERENCES

- [1] J. R. Uijlings, K. E. Van De Sande, T. Gevers, and A. W. Smeulders, "Selective search for object recognition," *International journal of computer vision*, vol. 104, no. 2, pp. 154–171, 2013.
- [2] J. Yang and J. Yuan, "Common action discovery and localization in unconstrained videos," in *The IEEE International Conference on Computer Vision (ICCV)*, Oct 2017.
- [3] O. P. Popoola and K. Wang, "Video-based abnormal human behavior recognition review," *IEEE Transactions on Systems, Man, and Cybernetics, Part C (Applications and Reviews)*, vol. 42, no. 6, pp. 865–878, Nov 2012.
- [4] L. Wang, D. Meng, X. Hu, J. Lu, and J. Zhao, "Instance annotation via optimal bow for weakly supervised object localization," *IEEE Transactions on Cybernetics*, vol. 47, no. 5, pp. 1313–1324, May 2017.
- [5] X. Zheng, R. Ji, X. Sun, Y. Wu, F. Huang, and Y. Yang, "Centralized ranking loss with weakly supervised localization for fine-grained object retrieval," in *IJCAI*, 2018, pp. 1226–1233.
- [6] L. Gao, J. Song, D. Zhang, and H. T. Shen, "Coarse-to-fine image co-segmentation with intra and inter rank constraints," in *IJCAI*, 2018, pp. 719–725.
- [7] K.-J. Hsu, Y.-Y. Lin, and Y.-Y. Chuang, "Co-attention cnns for unsupervised object co-segmentation," in *IJCAI*, 2018, pp. 748–756.
- [8] Z.-H. Yuan, T. Lu, and Y. Wu, "Deep-dense conditional random fields for object co-segmentation," in *IJCAI*, 2017, pp. 3371–3377.
- [9] M. Jain, H. Jegou, and P. Bouthemy, "Better exploiting motion for better action recognition," in *Computer Vision and Pattern Recognition (CVPR)*. IEEE, 2013, pp. 2555–2562.
- [10] H. Jiang, J. Wang, Z. Yuan, Y. Wu, N. Zheng, and S. Li, "Salient object detection: A discriminative regional feature integration approach," in *Computer Vision and Pattern Recognition (CVPR)*. IEEE, 2013, pp. 2083–2090.
- [11] K. R. Jerripothula, J. Cai, and J. Yuan, "Cats: Co-saliency activated tracklet selection for video co-localization," in *European Conference on Computer vision (ECCV)*. Springer, 2016, pp. 187–202.
- [12] S. Kwak, M. Cho, I. Laptev, J. Ponce, and C. Schmid, "Unsupervised object discovery and tracking in video collections," in *Proceedings of the IEEE International Conference on Computer Vision*. IEEE, 2015, pp. 3173–3181.
- [13] H. Wang, Y. Lai, W. Cheng, C. Cheng, and K. Hua, "Background extraction based on joint gaussian conditional random fields," *IEEE Transactions on Circuits and Systems for Video Technology*, vol. 28, no. 11, pp. 3127–3140, Nov 2018.
- [14] W. Wang, J. Shen, and L. Shao, "Consistent video saliency using local gradient flow optimization and global refinement," *IEEE Transactions on Image Processing*, vol. 24, no. 11, pp. 4185–4196, Nov 2015.
- [15] K.-Y. Chang, T.-L. Liu, and S.-H. Lai, "From co-saliency to co-segmentation: An efficient and fully unsupervised energy minimization model," in *Computer Vision and Pattern Recognition (CVPR)*. IEEE, 2011, pp. 2129–2136.
- [16] H. Fu, X. Cao, and Z. Tu, "Cluster-based co-saliency detection," *IEEE Transactions on Image Processing (T-IP)*, vol. 22, no. 10, pp. 3766–3778, 2013.
- [17] M. Sun, Z. Zhou, Q. Hu, Z. Wang, and J. Jiang, "Sg-fcn: A motion and memory-based deep learning model for video saliency detection," *IEEE Transactions on Cybernetics*, pp. 1–12, 2018.
- [18] W. Wang, J. Shen, H. Sun, and L. Shao, "Video co-saliency guided co-segmentation," *IEEE Transactions on Circuits and Systems for Video Technology*, vol. 28, no. 8, pp. 1727–1736, Aug 2018.
- [19] F. Guo, W. Wang, J. Shen, L. Shao, J. Yang, D. Tao, and Y. Y. Tang, "Video saliency detection using object proposals," *IEEE Transactions on Cybernetics*, vol. 48, no. 11, pp. 3159–3170, Nov 2018.
- [20] K. R. Jerripothula, J. Cai, and J. Yuan, "Quality-guided fusion-based co-saliency estimation for image co-segmentation and colocalization," *IEEE Transactions on Multimedia*, vol. 20, no. 9, pp. 2466–2477, Sep. 2018.
- [21] K. R. Jerripothula, J. Cai, and J. Yuan, "Image co-segmentation via saliency co-fusion," *IEEE Transactions on Multimedia*, vol. 18, no. 9, pp. 1896–1909, Sept 2016.
- [22] J. Lou, F. Xu, Q. Xia, W. Yang, and M. Ren, "Hierarchical co-salient object detection via color names," in *Proceedings of the Asian Conference on Pattern Recognition*, 2017, pp. 718–724. [Online]. Available: <http://www.loujing.com/hcn-co-sod/>
- [23] Z. Liu, W. Zou, L. Li, L. Shen, and O. Le Meur, "Co-saliency detection based on hierarchical segmentation," *IEEE Signal Processing Letters*, vol. 21, no. 1, pp. 88–92, Jan 2014.
- [24] P. Arbelaez, M. Maire, C. Fowlkes, and J. Malik, "Contour detection and hierarchical image segmentation," *IEEE Transactions on Pattern Analysis and Machine Intelligence*, vol. 33, no. 5, pp. 898–916, May 2011.
- [25] K. Tang, A. Joulin, L.-J. Li, and L. Fei-Fei, "Co-localization in real-world images," in *Computer Vision and Pattern Recognition (CVPR)*. IEEE, 2014, pp. 1464–1471.
- [26] K. R. Jerripothula, J. Cai, and J. Yuan, "Qcqe: Quality constrained co-saliency estimation for common object detection," in *Visual Communications and Image Processing (VCIP)*. IEEE, 2015, pp. 1–4.
- [27] M. Cho, S. Kwak, C. Schmid, and J. Ponce, "Unsupervised object discovery and localization in the wild: Part-based matching with bottom-up region proposals," in *Computer Vision and Pattern Recognition (CVPR)*. IEEE, 2015, pp. 1201–1210.
- [28] A. Joulin, K. Tang, and L. Fei-Fei, "Efficient image and video co-localization with frank-wolfe algorithm," in *European Conference on Computer vision (ECCV)*. Springer, 2014, pp. 253–268.
- [29] A. Prest, C. Leistner, J. Civera, C. Schmid, and V. Ferrari, "Learning object class detectors from weakly annotated video," in *Computer Vision and Pattern Recognition (CVPR)*. IEEE, 2012, pp. 3282–3289.
- [30] K. R. Jerripothula, J. Cai, and J. Yuan, "Efficient video object co-localization with co-saliency activated tracklets," *IEEE Transactions on Circuits and Systems for Video Technology*, vol. 29, no. 3, pp. 744–755, March 2019.
- [31] P. Tokmakov, K. Alahari, and C. Schmid, *Weakly-Supervised Semantic Segmentation Using Motion Cues*. Cham: Springer International Publishing, 2016, pp. 388–404.
- [32] A. Oliva and A. Torralba, "Modeling the shape of the scene: A holistic representation of the spatial envelope," *International journal of computer vision(IJCV)*, vol. 42, no. 3, pp. 145–175, 2001.
- [33] G. Guo, H. Wang, W. Zhao, Y. Yan, and X. Li, "Object discovery via cohesion measurement," *IEEE Transactions on Cybernetics*, vol. 48, no. 3, pp. 862–875, March 2018.
- [34] C. Rother, V. Kolmogorov, and A. Blake, "Grabcut: Interactive foreground extraction using iterated graph cuts," in *Transactions on Graphics (TOG)*, vol. 23, no. 3. ACM, 2004, pp. 309–314.
- [35] A. Vedaldi and B. Fulkerson, "VLFeat: An open and portable library of computer vision algorithms." <http://www.vlfeat.org/>, 2008.
- [36] F. Meng, H. Li, G. Liu, and K. N. Ngan, "Object co-segmentation based on shortest path algorithm and saliency model," *IEEE Transactions on Multimedia (T-MM)*, vol. 14, no. 5, pp. 1429–1441, 2012.